Hindawi
International Journal of Optics
Volume 2022, Article ID 1744180, 9 pages
https://doi.org/10.1155/2022/1744180

Research Article

Design of an Athermalizing Bonding Structure for Optical Components

Xiaofeng Liu, Xin Zhang, and Xindong Chen

Changchun Institute of Optics, Fine Mechanics and Physics, Chinese Academy of Sciences, Changchun 130033, China

Correspondence should be addressed to Xiaofeng Liu; liuxiaofengshen@163.com and Xin Zhang; zhangxin@tju.edu.cn

Received 26 October 2021; Revised 10 February 2022; Accepted 1 March 2022; Published 20 March 2022

Academic Editor: haochong huang

In this paper, an athermalizing connection method of the optical components of high-performance optical objectives that enables them to reduce the deterioration of their performance due to temperature instability is proposed. The optical components of the athermalizing connection structure consist of three parts arranged from the outside to the inside. The materials of the intermediate parts are different from those of the external and internal ones. The relationship between the parameters of the athermalizing connection structure is deduced based on the mechanics of materials. The surface errors of optical components at different temperatures are simulated for an exemplary structure. The simulation results show that the root mean square (RMS) of the optical component surface is approximately proportional to the temperature. When the temperature drops by 10 °C, the RMS changes by 0.66 nm as compared to its value measured at 20 °C. The temperature deflection test of the optical components carried out in the temperature range of 20 ± 5 °C provides the RMS values of the optical face of 0.019λ at 15 °C and 0.02λ at 25 °C. The change of RMS obtained in this test amounts to 0.63 nm for a temperature difference of 10 °C, which deviates from the respective simulated value by 4%. The experimental results show that the athermalizing connection method proposed in this paper ensures small deformations of optical components at large temperature changes. Therefore, it meets the requirements for the application of optical components and is suitable for the connection of high-precision components.

1. Introduction

High-performance optical objectives are the core elements of microscopic imaging and projection lithography equipment, which determine the performance of optical instruments [1–3]. Fine resolution and small aberration of objective lenses require high surface precision of optical components. The root mean square (RMS) of the surface roughness of some components needs to be 1% of the wavelength or less, and the surface stability should be maintained during the working process. In previous publications, a great number of designs of optomechanical structures have been proposed to ensure the stability of optical components [4–7].

Most optical elements are made of nonmetallic materials, and only a small number of reflective components are made of metals. In this paper, nonmetallic optical components are considered. Since such components cannot contain mounting holes, most of them are mounted by using optical adhesive. Linear expansion coefficients (LECs) of optical adhesives are generally one to two orders of magnitude higher than those of optical components. For example, the LEC of single crystalline Si is 2.6×10^{-6}/K, while that of optical epoxy adhesive (Bluestar Chengrand Co., Ltd.) is 70×10^{-6}/K. Such differences in LEC lead to the deformations of optical components with temperature changes.

Numerous methods have been proposed to eliminate the adverse effect of temperature on optical components. Liu Xiao-han et al. studied the support structure for the off-axis three-mirror astigmatism system with a size of 520 mm. The RMS change rate of this structure amounted to 0.117 nm/°C@100 mm [8]. Yu Fu-nan et al. studied a regular support structure for a hexagonal mirror with a size of 320 mm. In this case, the RMS change rate was 0.822 nm/°C@100 mm [9]. Yu Ji-chen et al. designed a back-supported mirror bonding structure with a diameter of 320 mm and an RMS change rate of 0.233 nm/°C@100 mm [10]. One may

conclude from previous studies that the values of the RMS change rate of optical components with flexible support structures of less than 0.05 nm/°C@100 mm (the characteristic value of the optical components considered in this paper) are difficult to achieve. Moreover, the described methods have limited applicability because the stiffness of the support structures is low and does not enable to eliminate the action of thermal stress on the optical components, which prevents the entire assembly from being used under strong shock vibration conditions.

In this paper, an athermalizing bonding structure, which is potentially suitable for applications in harsh mechanical environments and at large temperature variations, is proposed. The deformation mechanism of such structure is uncovered. Deformation of optical elements at different temperatures is analyzed by finite element analysis (FEA) method. Finally, a platform is established to test the proposed bonding structure. Obtained testing results demonstrate that this structure meets the requirements for high-performance optical objectives applications.

2. Principle of the Temperature Adaptability of Typical Bonding Structures

Adhesive bonding is a common way to install and fix optical components [11, 12]. The structure that is directly bonded to an optical component is usually referred to in engineering as a bushing. This term will be used in the next paragraphs to refer to the connection structure of optical components. Due to the difference in the thermal expansion coefficients of the optical component, adhesive layer, and bushing, thermal stress will appear between the optical component and the adhesive layer at the temperature change. This stress will result in a change of the surface shape of the optical component, which affects the optical performance of the whole system. Two methods may be applied to improve the temperature adaptability of optical components. The first one is to increase the stiffness of the connection points of optical components to resist the tensile stress caused by the adhesive layer. The other method implies a reduction of temperature stress by applying a proper bushing design.

Therefore, to reduce the adverse influence of temperature variation on the shape accuracy of a reflecting optical component, its stiffness at the connection point should be far greater than that of the bushing. In this case, the deformation of the optical components resulting from temperature change becomes much smaller than that of the bushing, and the former adapts well to temperature changes. Most of the supporting structures of optical components are designed based on this principle [13–20].

3. Athermalizing Design

It may be concluded from the previous section that the design of the bushing structure is the key factor for realization of the temperature adaptability of optical components. Adaptation of the thermal stress of optical components by using flexible bushing can be relied on at the working conditions implying slight temperature variations or low accuracy requirements. However, this approach is not suitable for significant temperature variations. An example of the flexible design of a typical optical component is shown in Figure 1. In this design, the flexible reed of the bushing is connected to the bonding structure. A significant change of working temperature causes deformation of the reed due to the inconsistency of LEC for the adhesive layer as well as the optical component and the bushing structure. Since good stiffness of the entire component is required, the deformation of the reed cannot fully adapt to the deformation of the adhesive layer. Therefore, an additional distribution force q(x) appears between the bushing and the adhesive layer in the opposite direction to bushing deformation. This force is transferred to the optical component through the adhesive layer resulting in the inability to adapt to significant temperature changes.

It is difficult to offset the force between the adhesive layer and the optical component because the LEC of the bushing should be equal to or greater than that of the adhesive layer for this, which is not the case for typical metal materials. Another way to solve this problem is to apply an extra reaction force to the bushing, which would balance the force between the adhesive and the optical component.

In view of these considerations, this paper proposes a design of a composite flexible cell structure with cross-distributed inner and outer rings, the principle of which is shown in Figure 2.

A cross-distributed bushing is composed of the outer ring, inner ring, and drive ring. When the temperature drops, this structure shrinks and deforms. As the LEC of the adhesive layer is much larger than that of the optical component and the bushing, deformation of the adhesive layer is partially suppressed by the optical component and the outer ring of the bushing. The deformation of optical element is shown in Figure 3, defining the amount of suppression as δ_a. If the material of the drive ring is different from that of the outer and inner rings of the bushing, and the LEC of the former is larger than that of the latter, shrinkage of the outer ring lags behind the one of the drive ring. At this point, the drive ring provides an additional inward deformation δ_d to the outer ring. When $\delta_a = \delta_d$, the optical component is not subjected to action of any additional force and its surface remains stable.

We carry out a theoretical analysis for a back-mounted mirror as an example. The geometric parameters of the bushing are shown in Figure 4. In order to simplify the design, the widths of the support bars of the inner and outer rings are set equal to each other. The thickness of the drive ring is t_4, the thermal expansion coefficients of the optical component is α_4, and Young's modulus of the optical component is E_4, respectively.

The deformation of the cell is shown in Figure 5. In this figure, the dotted line indicates the position of the bonding structure after deformation. When the optical component is kept in a low-temperature environment (below the assembly temperature), the adhesive layer provides a distributed force q to the outer ring. If the optical component is not subjected to thermal stress, q is equal to zero. The structure and the material characteristics of the drive ring are the key factors

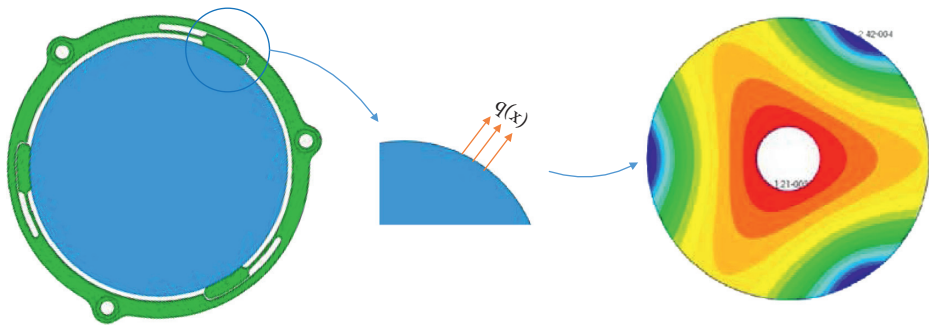

Figure 1: An example of flexible bushing.

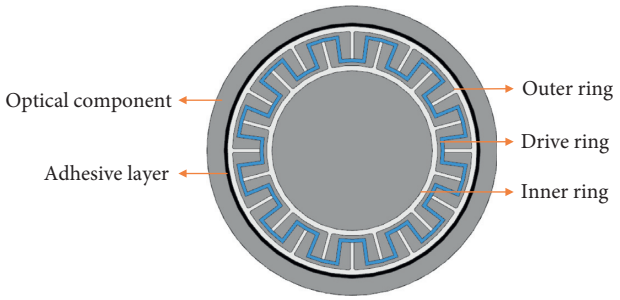

Figure 2: Cross-distributed combination bushing structure.

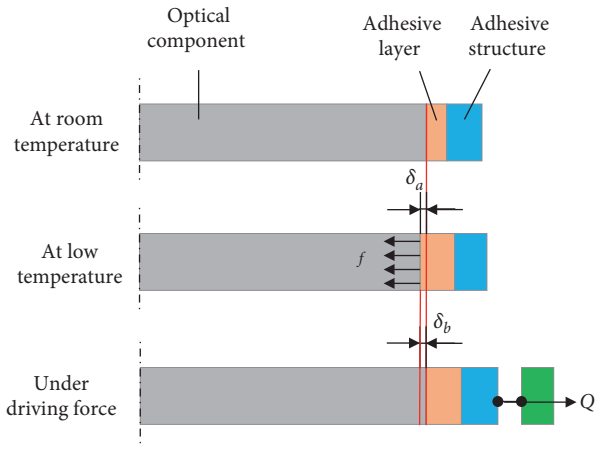

Figure 3: Deformation of optical component at low-temperature.

that enable to achieve this condition. The LEC of the drive ring should be greater than that of the inner and outer rings. In this way, the drive ring can provide a counterforce F_1 that offsets the distributed force q.

The radial force acting on the drive ring, F_2, can be obtained from geometric relations as $F_2 = 2F_1 cos\theta$.

Analysis of the forces acting on the cell structure presented previously enables to understand that the support ribs AB and EF are stretched, while the rib CD is compressed. We define δ_1, δ_2, δ_3, δ_4, and δ_5 to be the deformations of the inner ring of the bushing, support rib of the inner ring, radial spring of the drive ring, support rib of the outer ring and the outer ring, respectively.

When the temperature drops by ΔT,

$$OE' = OF' + F'E' = \left(\frac{d}{2} + l_1\right)(1 - T \cdot \alpha_2) - \delta_1 - \delta_2, \quad (1)$$

$$OB' = \left(\frac{D}{2} - l_3\right)(1 - T \cdot \alpha_2) + \delta_5 + \delta_4. \quad (2)$$

Taking into account that $C'D' = OC' - OD' = (OE' - OB')$, the following expression is obtained:

$$C'D' = \left(\frac{d}{2} + l_1 + l_3 - \frac{D}{2}\right)(1 - T \cdot \alpha_2) - \delta_1 - \delta_2 - \delta_4 - \delta_5. \quad (3)$$

$l_2 = OE - OB = ((d/2) + l_1 + l_3 - (D/2))$, which enables to simplify expression (3) as follows:

$$C'D' = l_2(1 - T \cdot \alpha_2) - \delta_1 - \delta_2 - \delta_4 - \delta_5. \quad (4)$$

Since thermal deformation of the radial reed of the drive ring is δ_3, the length $\overset{\frown}{C'D'}$ can be expressed as follows:

$$C'D' = l_2(1 - T \cdot \alpha_3) - \delta_3. \quad (5)$$

Combination of two equations presented previously results in the following expression:

$$\delta_1 + \delta_2 - \delta_3 + \delta_4 + \delta_5 = l_2 \Delta T(\alpha_3 - \alpha_2). \quad (6)$$

According to the deformation theory of the mechanics of materials,

$$\delta_1 = \frac{F_1 d}{2E_2 \theta h t_1}, \quad (7)$$

$$\delta_2 = \frac{2F_1 l_1}{E_2 h t_3}, \quad (8)$$

$$\delta_3 = \frac{F_1 l_2 cos\theta}{E_3 h t_4}, \quad (9)$$

$$\delta_4 = \frac{2F_1 l_3 cos\theta}{E_2 h t_3}, \quad (10)$$

$$\delta_5 = \frac{F_1 D cos\theta}{2E_2 \theta h t_2}. \quad (11)$$

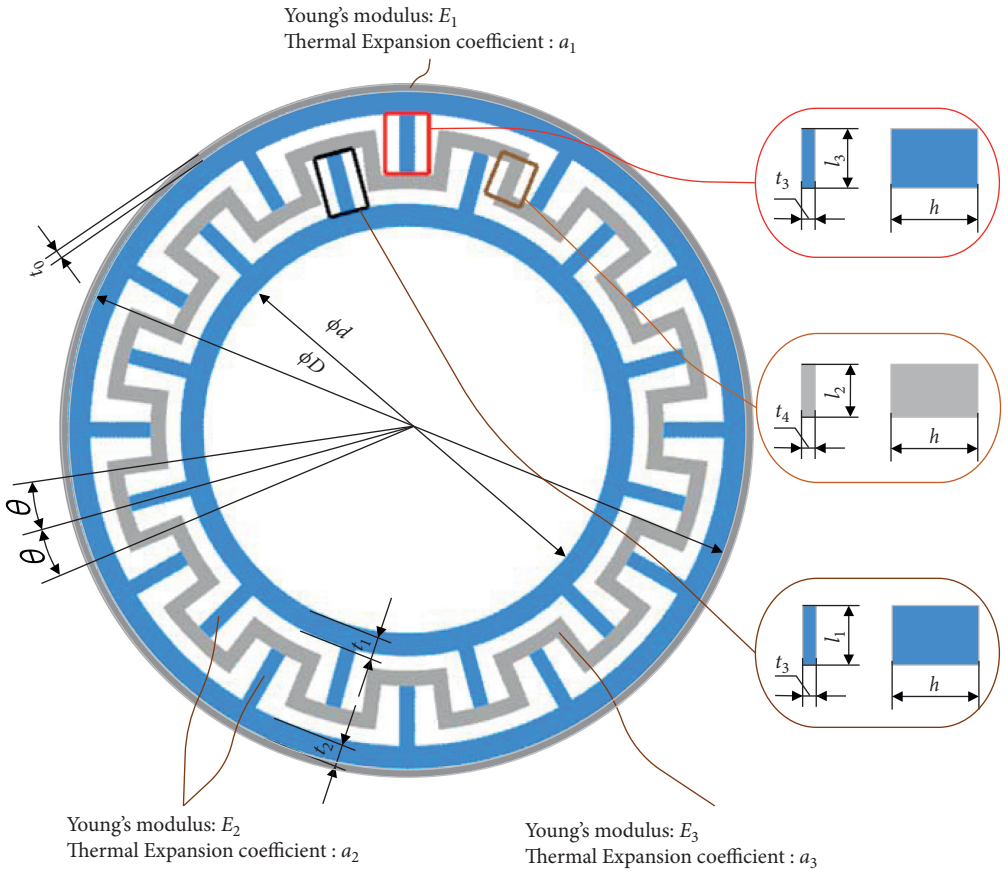

Figure 4: Geometric parameters of flexible intercrossing bushing.

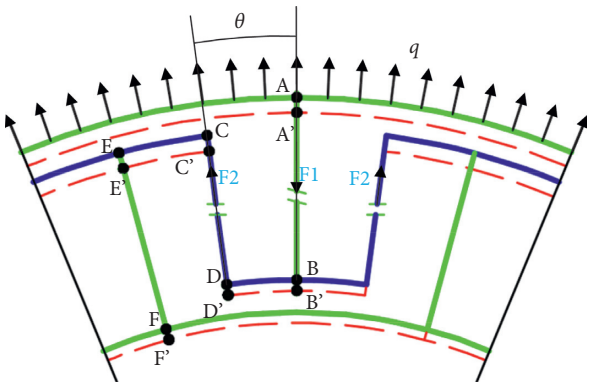

Figure 5: Cell deformation diagram of bushing.

When the number of cells $n \geq 12$, $cos\theta = cos(\pi/n) \approx 1$. Substituting equations (7) and (11) into (6), one obtains

$$\frac{F_1}{E_2 h}\left(\frac{d}{2\theta t_1}+\frac{D}{2\theta t_2}-\frac{E_2 l_2}{E_3 t_4}+\frac{2l_1+2l_3}{t_3}\right)=l_2\Delta T(\alpha_3-\alpha_2). \tag{12}$$

When the ratio of the diameters and the thicknesses of the inner and the outer rings is much greater than the thickness ratio of the support rib and the drive reed, $(d/2\theta t_1)+(D/2\theta t_1) \gg (2l_1+2l_3/t_3)-(E_2 l_2/E_3 t_4)$. This is equivalent to $\delta_1+\delta_5 \gg \delta_2-\delta_3+\delta_4$ and hence

$$\delta_1+\delta_5=l_2\Delta T(\alpha_3-\alpha_2). \tag{13}$$

After the temperature of the ring changes, the distance between the inner and the outer rings becomes

$$\Delta r_{\text{inner-outer}}=\frac{1}{2}(D-d)\alpha_2\Delta T-\delta_1-\delta_5. \tag{14}$$

The LEC of the optical component is very small as compared to that of the adhesive layer, and the distortion of the mirror is negligible. Therefore, the thickness of the adhesive layer changes to

$$\Delta r_{\text{adhesive}} \approx t_0\alpha_1\Delta T. \tag{15}$$

Due to the constraint on the inner ring, the condition for compensating the change in the thickness of the adhesive layer, $\Delta r_{\text{inner-outer}}=\Delta r_{\text{adhesive}}$, should be met, which results in the following expression:

$$\frac{1}{2}(D-d)\alpha_2\Delta T-\delta_1-\delta_5=t_0\alpha_1\Delta T. \tag{16}$$

The following equation can be obtained from expressions (15) and (19):

$$l_2=\frac{1}{2}(\mathrm{D}-\mathrm{d})\frac{\alpha_2}{\alpha_3-\alpha_2}-\frac{t_0\alpha_1}{\alpha_3-\alpha_2}. \tag{17}$$

When (17) is satisfied, the bushing can keep the shape of the surface of the optical component stable. Of course, the latter expression was obtained with some simplifications. Therefore, the athermalizing structure proposed in this paper is an approximate one.

It can be seen that the selection of bushing material is the key factor in athermalizing design. In addition, the deformation of the bushing is related to strength and Young's modulus. The maximum deformation of the material δ_{max} depends on the allowable stress σ_s and Young's modulus E, which is expressed as follows:

$$\delta_{max} = k\frac{\sigma_s}{E}. \tag{18}$$

The factor k depends on the cross-sectional area of the structure. Due to the large deformation of the support ring to offset the reaction force produced by the adhesive layer, the material of the drive ring has higher requirement for δ_{max} as compared to that of the inner and outer rings. Table 1 shows the parameters of the materials commonly used for drive rings.

As can be seen from Table 1, the value of δ_{max} for titanium alloy is the largest one. Therefore, this alloy was selected as the drive ring material. As abovementioned, the LEC of the support ring should be larger than that of the inner and outer rings. In this respect, invar alloy has been selected as the material for the latter.

The parameters of the mirror in this example are shown in Table 2.

The value $l_2 \approx 2.3$ mm is obtained by calculation. The athermalizing bushing structure designed according to the structural parameters of the bushing is shown in Figure 6.

Table 1: Elastic material parameters commonly used.

Materials	σ_s (MPa)	E (GPa)	LEC (10^{-6}/K)	δ_{max}
Invar alloy	470	138	0–3	3.4
Titanium alloy	877	117	9.1	7.5
2Cr13	835	228	10.5	3.7
Aluminum	210	69	23.9	3
Copper	328	99	18	3.3
Magnesium alloy	160	45	25	3.56

Table 2: Parameters of the mirror.

Materials	Value
D	66 mm
d	52 mm
α_2	2.5×10^{-6}/K
t_0	0.04 mm
α_1	70×10^{-6}/K
l_1	2.2 mm
α_3	9.1×10^{-6}/K
l_3	2.2 mm
θ	15°

4. Finite Element Analysis

To prove the validity of the theory developed in this paper, FEA was carried out on the athermalizing structure. The adhesive layer should have sufficient mesh resolution to simulate its elastic behavior. For this reason, the element type was chosen to be tetrahedral, and the number of elements was 48932. The outer cylinder of the adhesive layer was bonded to the optical components, and the inner cylinder was bonded to the outer ring of the bushing, respectively.

The operation temperature of the optical element studied in this paper is 20 °C ± 3 °C, and the environment temperature during its storage and transportation is 20 °C ± 10 °C. The RMS changes by less than 2 nm at mentioned temperatures, and the RMS change rate is less than 0.05/°C@100 mm. In order to test whether the athermalizing structure can adapt to a wider temperature range, the simulation temperature gradient was extended to 20°C, which is denoted here as δ20 °C. The analysis was carried out for the temperature variations of δ3°C, δ10 °C, and δ20 °C relative to the reference value of 20 °C corresponding to the room temperature. The optical component material was single-crystalline Si and the adhesive was an optical epoxy resin. The thickness of the adhesive layer was 0.04 mm. The material of the outer ring of the liner and the inner ring was invar alloy, and the material of the drive ring was titanium alloy. Patran/Nastran software was used for finite element analysis, and surface shape calculations were performed using MATLAB. The results of the analysis are shown in Table 3. Figure 7 presents the deformation results of the mirror assembly at a temperature drop of δ10 °C.

As can be seen from the results of calculations presented in Table 3, the optical component bonded to the athermalizing structure can accommodate a wider temperature range as compared to traditional structures mentioned in section 1. The RMS change rate of the optical component in the athermalizing design structure is calculated to be 0.033 nm/°C@100 mm. Obtained results demonstrate that the proposed design meets the high-precision requirements of objective lenses.

5. Experimental Verification

It is very difficult to measure the surface shape of optical components, especially aspherical ones, under extreme temperature conditions. According to the principle of aspherical surface testing presented in Figure 8, an optical element is placed in a low-temperature liquid nitrogen tank or a heating cage, and a compensator is placed outside. The distance between the optical element and the compensator is usually fixed and not large. The liquid nitrogen tank or the heating cage must separate the optical element from the compensator to ensure that the latter is in a normal working environment. At this, a low- or high-temperature environment should be set for the optical component. Therefore, the tank or the cage needs to make use of the entire space between the compensator and the optical component. Moreover, a window should be placed in this space to maintain the temperature stability in the tank. The performance of the window is not affected by the temperature in the liquid nitrogen tank or heating cage that is difficult to

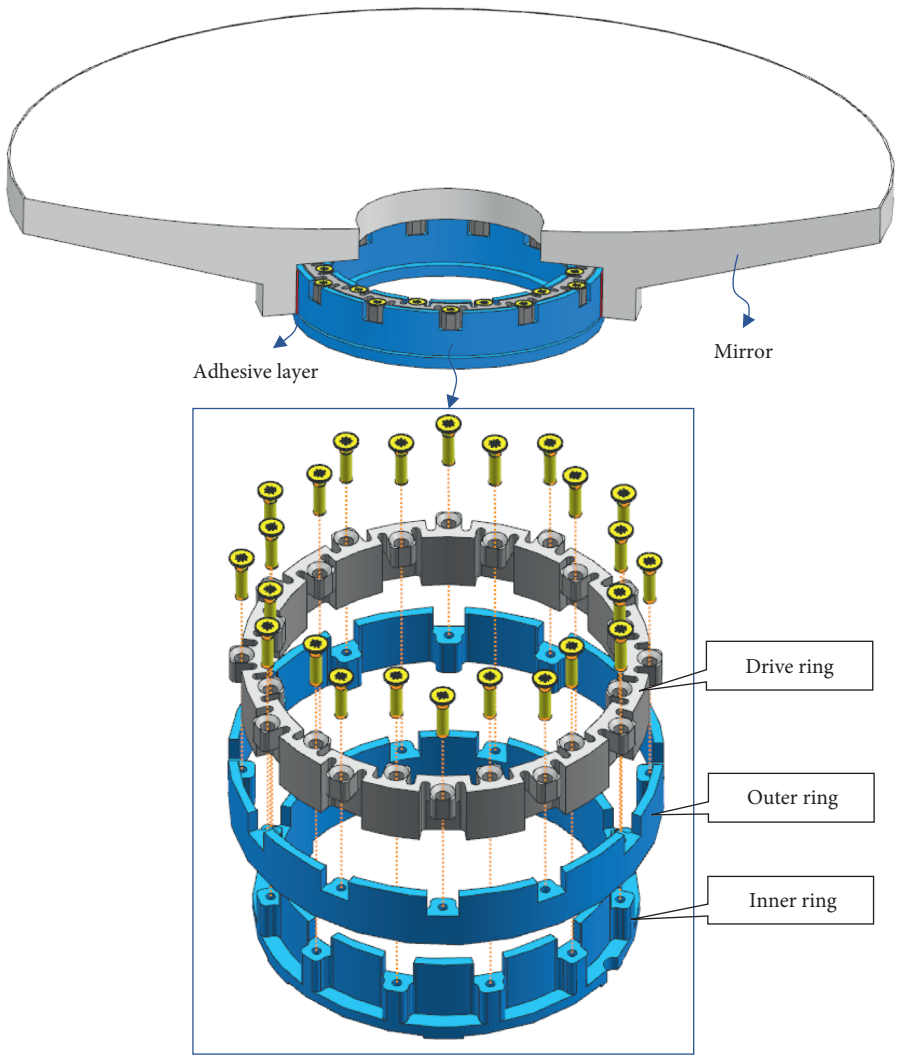

Figure 6: Athermalizing bushing construction.

Table 3: FEA results.

Temperature drop	PV/nm	RMS/nm
$\delta 3$ ˚C	1.76	0.20
$\delta 10$ ˚C	5.82	0.66
$\delta 20$ ˚C	11.19	1.25

achieve. In view of the complexity of this problem, some researchers studied wave aberration under extreme temperatures. However, there are limitations on the testing conditions and accuracy [21, 22].

The most effective method of the performance evaluation of optical components at temperatures different from the room one, is to change the ambient temperature without affecting the accuracy of the detection tool. Specifically, placing the detector and the optical component assembly in a test chamber where temperature can be controlled and then measuring the RMS value of the optical component at

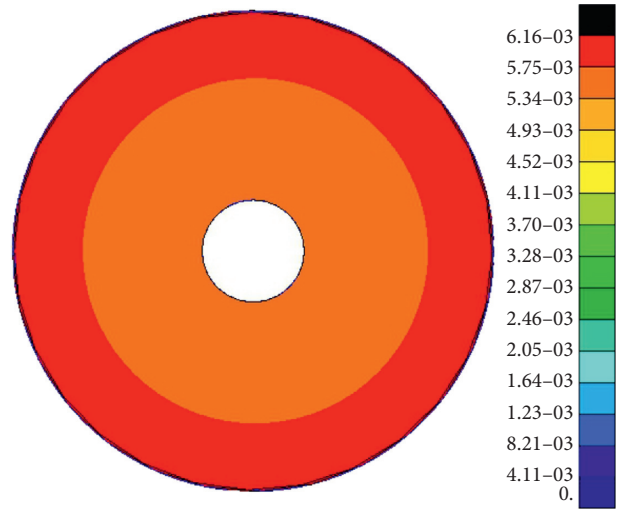

Figure 7: Deformation of mirror at the temperature drop of $\delta 10$ ˚C.

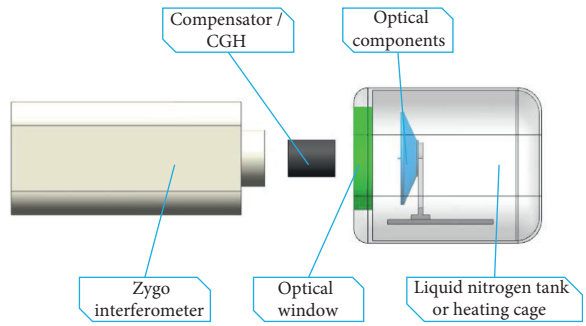

Figure 8: Detection principle of optical component surface shape.

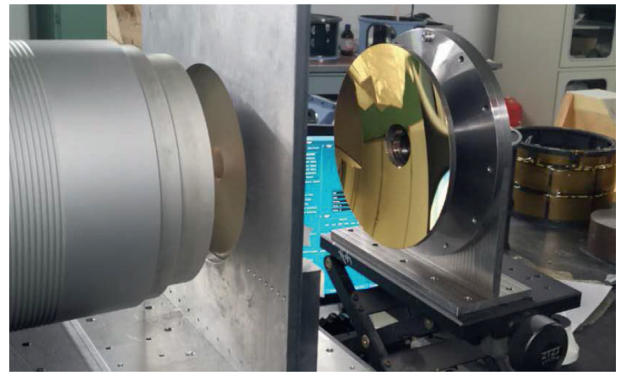

Figure 9: The surface detection process under the temperature deflection test.

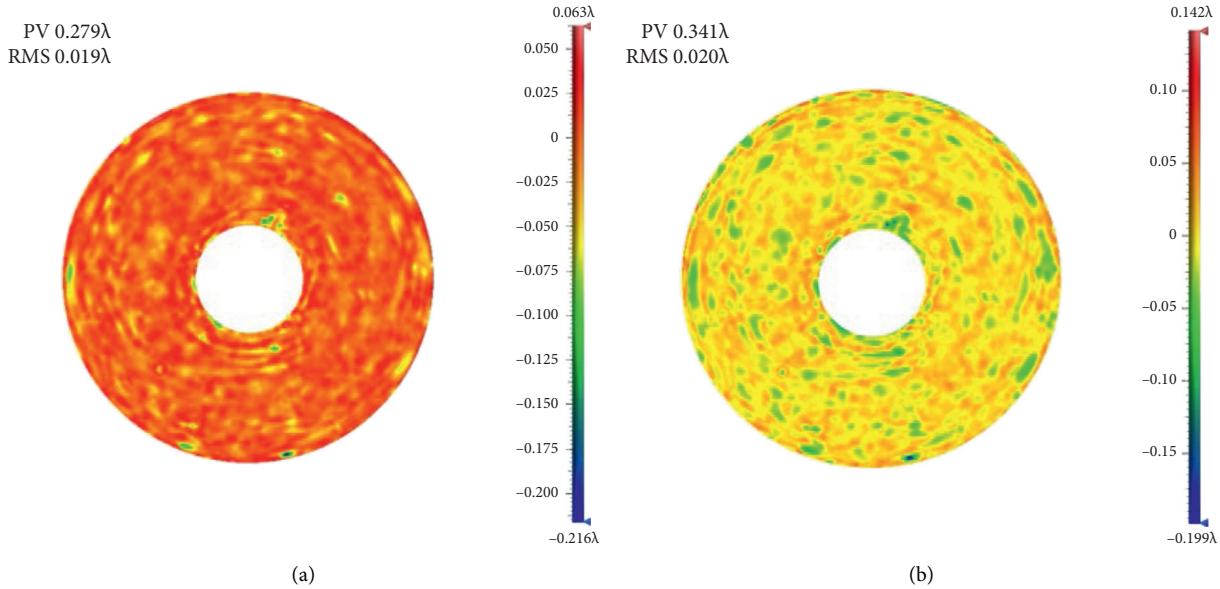

Figure 10: Temperature deflection test results. (a) Test results at 15 ˚C. (b) Test results at 25.

different temperatures to evaluate the effectiveness of the bonding structure.

The accuracy of the detector at different temperatures is also an important reason for the introduction of detection errors. The operating temperature range of the Zygo verifier used in our experiments is 15 to 30 ˚C, and the allowable temperature change rate is below 1 ˚C/15 min. Therefore, the planned measurement temperature range was from 15 to 25 ˚C (20 ˚C ± 5 ˚C) to exclude the influence of the verifier on the detection accuracy.

Before the test, the athermalized bonding structure proposed in this paper was mounted on the optical component. The optical component was subjected to sufficient thermal cycling to exclude the influence of thermal stress on the test results.

The test was carried out as follows. First, the detection optical path of the optical component was set up at room temperature (20 ˚C). After that, the temperature in the laboratory was lowered to 15 ˚C at a cooling rate of 1 ˚C/30 min. This temperature was kept for a period of 24 hours so that the optical element assembly could fully accommodate it. Then, the RMS value of the optical element was measured by the Zygo interferometer. After completion of detection, the temperature was raised to 30 ˚C at a heating rate of 1 ˚C/30 min. The RMS value of the optical component was measured again after maintaining this temperature for 24 hours. Finally, the test results were processed.

The detection process is shown in Figure 9. The results of the testing are presented in Figure 10.

The optical axis of the mirror is horizontal when it is working, and the optical axis of the mirror is kept horizontal in the process of processing and detection. Once the aberration in the direction of gravity is detected, it will be removed during optical processing, so the influence of gravity cannot be reflected in the detection result.

The experimental RMS values of the optical element are 0.019λ at 15 ˚C and 0.020λ at 25 ˚C. The testing wavelength is 632.8 nm. When the temperature changes by 10 ˚C, the RMS value changes by 0.63 nm. The experimental results deviate from the respective FEA results by 4%. The RMS change rate is 0.0315 nm/˚C@100 mm, which meets the requirements for high-performance optical objective applications.

6. Conclusion

In this paper, an athermalizing bonding structure, which meets strict requirements for temperature adaptability of high-precision optical components, is proposed. The athermalizing design structure of the optical component is verified theoretically. The surface errors of optical components are simulated at different temperatures for an exemplary structure. The simulation results show that the RMS of the optical component changes by 0.66 nm at a temperature change of 10˚C. In order to verify the correctness of the theoretical analysis, the temperature deflection test of the optical component was carried out for the deflection temperature range of 20 ± 5˚C. The RMS value of the surface shape is found to be $0.019\ \lambda$ at 15 ˚C and $0.02\ \lambda$ at 25 ˚C. The RMS of the optical component changes by 0.63 nm at a temperature change of 10˚C. The experimental results deviate from the simulation ones by 4%. The results of theoretical analysis and experimental tests show that the athermalizing bonding structure proposed in this paper can enable to improve low-temperature adaptability of optical components. These results have guiding significance for the high-precision objective installation.

Data Availability

The data are included within the manuscript.

Conflicts of Interest

The authors declare that they have no conflicts of interest.

Acknowledgments

The Bethune Center for Medical Engineering and Instrumentation in Jilin Province, China, actively supported this study. The project number is BQEGCZX2019032. The authors would like to express their gratitude to EditSprings (https://www.editsprings.com/) for the expert linguistic services provided.

References

[1] Y.-F. Dai and X.-Q. Peng, "Overview of key technologies for optical manufacturing of lithographic projection lens," *Journal of Mechanical Engineering*, vol. 49, no. 4, pp. 10–18, 2013.

[2] J. Lei, S.-L Jiang, and G. Cheng, "Deformation of high-accuracy photolithographic objective lens," *Opto-Electronic Engineering*, vol. 32, no. 2, pp. 12–14, 2005.

[3] Y.-Y Hua and Y. Gong, "Design and analysis for the high-precision lens flexible structure of lithography objective lens," *Opto-Electronic Engineering*, vol. 40, no. 7, pp. 39–43, 2013.

[4] X. Liu, X. Tian, W. Zhang et al., "Lightweight design of high volume SiC/Al composite mirror for remote camera," *Optik*, vol. 188, pp. 64–70, 2019.

[5] L. Zhang, W. Wang, J. Wang, P. Guo, and L. Hao, "Design and analysis for the multi-point flexible support structure of large and precision lens," *Optik*, vol. 193, p. 162966, 2019.

[6] K.-J Wang, J.- H Dong, and X.-Y Wang, "Design of frame-type support structure for space-based rectangular convex mirror tested on the back," *Optik*, vol. 212, Article ID 164673, 2020.

[7] D. Vukobratovich and R. M. Richard, "Flexure mounts for high-resolution optical elements," *SPIEL*, vol. 959, pp. 17–36, 1988.

[8] X.-H Liu, S.-C Li, and M.-X Li, "Supporting structure design for primary and tertiary mirror of off-axis TMA system," *Infrared and Laser Engineering*, vol. 50, no. 8, Article ID 20210025, 2021.

[9] F.-N Yu and C.-Y Zhang, "Support structure design of a hexagonal reflect mirror," *Journal of Changchun University of Science and Technology (Natural Science Edition)*, vol. 43, no. 3, pp. 1–6, 2020.

[10] Y. Jichen, Y. Jian, L. Mingxuan, and Y. Xuezhi, "Design of adhesive structure for back-supported space reflector inserts," *Acta Optica Sinica*, vol. 39, no. 5, Article ID 0523002, 2019.

[11] Y. Wen-jie and L. Xuan, "Using the equivalent stress to analyze the effect of temperature change on surface accuracy of the bonded mirror," *Acta Photonica Sinica*, vol. 44, no. 12, Article ID 1212001, 2015.

[12] M.-Q Li, L. Zhang, and L.-N Xing, "Optimization design of athermal adhesive for rectangular space mirror," *Chinese Optics*, vol. 9, no. 6, pp. 704–712, 2016.

[13] L. Zhang, T. Wang, F. Zhang, H. Zhao, Y. Zhao, and X. Zheng, "Design and optimization of integrated flexure mounts for unloading lateral gravity of a lightweight mirror for space application," *Applied Optics*, vol. 60, no. 2, pp. 417–426, 2021.
[14] M. Shao, L. Zhang, and X. Jia, "Optomechanical integrated optimization of a lightweight mirror for space cameras," *Applied Optics*, vol. 60, no. 3, pp. 539–546, 2021.
[15] H. Kihm and H. Yang, "Design optimization of a 1-m lightweight mirror for a space telescope," *Optical Engineering*, vol. 52, no. 9, Article ID 091806, 2019.
[16] B. Liu, W. Wang, Y.-J. Qu, X.-P. Li, X. Wang, and H. Zhao, "Design of an adjustable bipod flexure for a large-aperture mirror of a space camera," *Applied Optics*, vol. 57, no. 15, pp. 4048–4055, 2018.
[17] R. Hu, S. Liu, and Q. Li, "Topology-optimization-based design method of flexures for mounting the primary mirror of a large-aperture space telescope," *Applied Optics*, vol. 56, no. 15, pp. 4551–4560, 2017.
[18] Y.-C. Chen, B.-K. Huang, Z.-T. You, C.-Y. Chan, and T.-M. Huang, "Optimization of lightweight structure and supporting bipod flexure for a space mirror," *Applied Optics*, vol. 55, no. 36, pp. 10382–10391, 2016.
[19] H. Kihm, H.-S. Yang, I. K. Moon, J.-H. Yeon, S.-H. Lee, and Y.-W. Lee, "Adjustable bipod flexures for mounting mirrors in a space telescope," *Applied Optics*, vol. 51, no. 32, pp. 7776–7783, 2012.
[20] W.-C Lin, S.-T Chang, and S.-H Chang, "Alignment and assembly process for primary mirror subsystem of a space-borne telescope," *Optical Engineering*, vol. 54, no. 11, Article ID 115109, 2015.
[21] Q.-Q Peng, S.-J Luo, and W.-B He, "Assembling and alignment of cryogenic optical system at room temperature based on phase compensation," *Laser & Infrared*, vol. 43, no. 4, pp. 433–437, 2013.
[22] H. Katayama, Y. Yamamoto, and M. Miyamotob, "Measurement of vibration environment of 6m diameter radiometer thermal vacuum chamber in JAXA," *SPIEL*, vol. 7436, Article ID 74360Q, 2009.